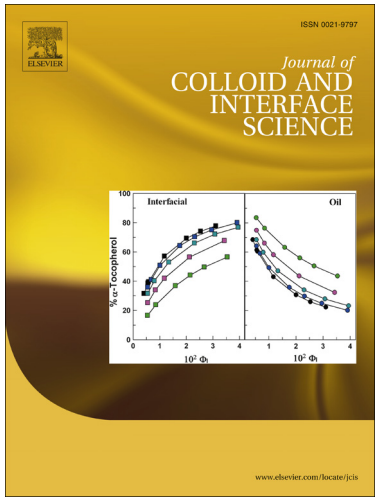

Effective fingerprint recognition technique using doped yttrium aluminate nano phosphor material

G.P. Darshan, H.B. Premkumar, H. Nagabhushana, S.C. Sharma, S.C. Prashanth, B. Daruka Prasad

PII: S0021-9797(15)30335-0
DOI: http://dx.doi.org/10.1016/j.jcis.2015.11.025
Reference: YJCIS 20876

To appear in: *Journal of Colloid and Interface Science*

Received Date: 19 September 2015
Revised Date: 11 November 2015
Accepted Date: 12 November 2015

Please cite this article as: G.P. Darshan, H.B. Premkumar, H. Nagabhushana, S.C. Sharma, S.C. Prashanth, B. Daruka Prasad, Effective fingerprint recognition technique using doped yttrium aluminate nano phosphor material, *Journal of Colloid and Interface Science* (2015), doi: http://dx.doi.org/10.1016/j.jcis.2015.11.025

Effective fingerprint recognition technique using doped yttrium aluminate nano phosphor material

GP Darshan[1, 2], H B Premkumar[3*], H Nagabhushana[4*], S C Sharma[5], S C Prashanth[6], B. Daruka Prasad [7]

[1]Department of Physics, Acharya Institute of Graduate Studies, Bangalore 560 107, India
[2]Research and Development Center, Bharathiar University, Coimbatore 641046, India
[3]Department of Physics, Dayananda Sagar Academy of Technology and management, Bangalore 560082, India
[4]Center for Nano Research (CNR), Tumkur University, Tumkur 572 103, India
[5]**Dayananda Sagar University,** Shavige Malleshwara Hills, Bangalore- 560078, India
[6]Department of Science, East West Institute of Technology, Bangalore 560 091, India
[7]Department of Physics, BMS Institute of Technology, VTU- affiliated, Bangalore-560 064, India

Abstract

First time the yttrium aluminate nanoparticles are used to improve the fingerprint quality. Eco-friendly green combustion process is used to synthesize $YAlO_3:Sm^{3+}$ (0.5 - 11 mol %) nanophosphor using green tea leaf extract as non-toxic and eco-friendly fuel. Powder X-ray diffraction study confirms the orthorhombic phase. The average sizes of the crystallites were found to be in the range 20 - 35 nm. The emission peaks centered at 564, 601 and 647 nm is attributed to 4f-4f $\left({}^4G_{5/2} \rightarrow {}^6H_{J=5/2,\,7/2,\,9/2}\right)$ forbidden transitions of Sm^{3+} ions. Judd-Ofelt theory is applied to experimental data for providing qualitative support by determining J-O intensity parameters. The Commission International De I-Eclairage chromaticity co-ordinates are very close to National Television System Committee standard value of white emission(x = 0.296, y = 0.237). Further, correlated color temperature is found to be ~11900 K. A simple, fast, highly sensitive and low-cost method for the detection and enhancement of fingermarks in a broad range of surfaces is developed and constitutes an alternative to traditional luminescent powders.

Keywords: Nanophosphor; Photoluminescence; Fingerprint detection; Solution combustion.

* Corresponding authors. Tel.: +91-9880433880, E-mail: premhb@gmail.com (HB Premkumar)
+91- 9945954010, E-mail: bhushanvlc@gmail.com (H. Nagabhushana)

Highlights

- First time $YAlO_3:Sm^{3+}$ nanophosphor was used to improve the quality of finger print.
- Ecofriendly green combustion process is used to synthesize nanophosphor.
- CIE values of the samples were close to NTSC standard values of white emission.
- Enhancement of fingermarks recognition was achieved by simple and quick method.

Effective fingerprint recognition technique using doped yttrium aluminate nano phosphor material

GP Darshan[1, 2], H B Premkumar[3*], H Nagabhushana[4*], S C Sharma[5], S C Prashanth[6], B. Daruka Prasad [7]

[1]*Department of Physics, Acharya Institute of Graduate Studies, Bangalore 560 107, India*
[2]*Research and Development Center, Bharathiar University, Coimbatore 641046, India*
[3]*Department of Physics, Dayananda Sagar Academy of Technology and management, Bangalore 560082, India*
[4]*Center for Nano Research (CNR), Tumkur University, Tumkur 572 103, India*
[5]*Dayananda Sagar University, Shavige Malleshwara Hills, Bangalore- 560078, India*
[6]*Department of Science, East West Institute of Technology, Bangalore 560 091, India*
[7]*Department of Physics, BMS Institute of Technology, VTU- affiliated, Bangalore-560 064, India*

Abstract

First time the yttrium aluminate nanoparticles are used to improve the fingerprint quality. Eco-friendly green combustion process is used to synthesize $YAlO_3:Sm^{3+}$ (0.5 - 11 mol %) nanophosphor using green tea leaf extract as non-toxic and eco-friendly fuel. Powder X-ray diffraction study confirms the orthorhombic phase. The average sizes of the crystallites were found to be in the range 20 - 35 nm. The emission peaks centered at 564, 601 and 647 nm is attributed to 4f-4f $\left({}^4G_{5/2} \rightarrow {}^6H_{J=5/2,\,7/2,\,9/2}\right)$ forbidden transitions of Sm^{3+} ions. Judd-Ofelt theory is applied to experimental data for providing qualitative support by determining J-O intensity parameters. The Commission International De I-Eclairage chromaticity co-ordinates are very close to National Television System Committee standard value of white emission(x = 0.296, y = 0.237). Further, correlated color temperature is found to be ~11900 K. A simple, fast, highly sensitive and low-cost method for the detection and enhancement of fingermarks in a broad range of surfaces is developed and constitutes an alternative to traditional luminescent powders.

Keywords: Nanophosphor, Photoluminescence, Fingerprint detection, Solution combustion

* Corresponding authors. Tel.: +91-9880433880, E-mail: premhb@gmail.com (HB Premkumar)
+91- 9945954010, E-mail: bhushanvlc@gmail.com (H. Nagabhushana)

1. Introduction

Fingerprint acts as the most authoritative tool for categorizing people since the ridge patterns of every print is sole and unchallengeable. Latent fingerprints are one type of invisible prints that need a development for visualization and identification. For fixed surfaces at a crime scene, powdering residues the main physical fingerprint detection method. The fingerprint powder is categorized into three types: regular, metallic, and luminescent. Regular finger print powder contains of a resinous polymer for adhesion and a colorant for contrast. However, in Metallic powders containing meshed metals are used. Conventional fingerprint powders are incapable to develop latent detection on certain hard surfaces and mostly based on hazard metallic compound to the user's health [1]. However, the commercial particles used were not well dispersed and uniform in shape, having a large size range from ~0.2 to 2 μm. Such large particles with non-uniform shapes could interfere with the affinity between the particles and the finger marks; even detailed features of the finger marks, such as sweat pores, could be covered by the larger particles, leading to decreased detection sensitivity. Hence a uniform spherical shaped morphology is required for fingerprint detection. To overcome such restrictions is using powder-based on luminescent nano-materials. Recently, luminescent based nano-powders are explored as a potential elucidation to complications facing fingerprint detection. In addition, the size of the powder particles has a large effect on the adhesion effectiveness to fingerprint. In general, fine particles adhere better than larger ones. So using aluminate based nanopowders as labeling agents in fingerprint detection has stimulated the Material scientists.

Trivalent rare-earth ions-activated aluminate phosphors have attracted great prominence for white light-emitting diodes (WLEDs) in solid-state lighting applications due to their stability and environmentally friendly in comparison with sulfides [2 - 6]. Particularly, phosphor-

converted WLEDs which operate in the wavelength range of 350 - 420 nm are being considered as the most promising white-light source due to energy saving, long lifetime, and environmental-friendly nature in comparison with conventional light bulbs [7 - 10]. A typical pc-WLED is made up of blue LED covered with yellowish-green phosphor or a combination of red and green phosphors [11 -13]. The WLEDs with yellowish-green phosphor lack the red region emission [14]. In WLEDs with red and green phosphors, the luminescence efficiency is very much affected by the reabsorption of blue light by the phosphors and similarly in near ultraviolet (NUV)/UV excitation-based WLEDs [15]. In this view, efficient white-light emission can be expected from full color emitting single phase phosphors with co-excited activators [16].

Luminescence of materials are highly depends on their electronic band structure. Rare Earth (RE) element ions in divalent/ trivalent state have intense luminescence because of 4f electron transitions. Hence, luminescence of RE elements is almost independent of the host matrix. However, the energy levels of RE elements could be largely influenced by the crystal symmetry, and which is depending on the host material. Therefore, the choice of suitable material is a very important factor for achieving better optical properties [17, 18].On the other hand Aluminum–Yttrium oxides such as Al-rich cubic $Y_3Al_5O_{12}$ (YAG), Y-rich monoclinic $Y_4Al_2O_9$ (YAM) and a metastable hexagonal phase (YAH) with the same $YAlO_3$ (YAP) stoichiometry are well recognized as crucial class of materials for advanced optical technologies [19 - 22]. YAP is considered as the ideal alternate for YAG in many aspects. It has been widely used as host matrix for laser and phosphors, such as Nd^{3+} doped $YAlO_3$ [23], Tb^{3+}-doped $YAlO_3$ [24], $Yb^{3+}/Er^{3+}/Tm^{3+}$- tri-doped $YAlO_3$ nanocrystalline [25] etc. However, $YAlO_3$ is a metastable form in the Y_2O_3–Al_2O_3 system and has three forms itself: hexagonal, orthorhombic and cubic [26]. Among the RE^{3+} ions, Sm^{3+} ions are excellent activators to produce orange or reddish

emission from different inorganic host lattice [27]. Recently Sm^{3+} doped with different host lattice has been well documented [28-30]. Therefore, in the present work, YAP: Sm^{3+} (0.5-11 mol %) phosphors has been synthesized by a combustion route and well characterized by means of XRD, SEM, TEM, FT-IR, UV-Vis and PL.

2. Experimental

Fresh green tea leaves were collected from the local market of Tumkur, India. The cleaned green tea leaves were dried in the sun for 2 days. The dry leaves became crispy and were crashed by hand. Yttrium nitrate [$Y(NO_3)_3.4H_2O$ (99.9%)], Aluminum nitrate [$Al(NO_3)_3.9H_2O$ (99.9%)] and Samarium nitrate [$Sm(NO_3)_3$ (99.9%] were received from Sigma-Aldrich chemicals Ltd. All these chemicals were used as received and for all experimental work, doubly deionized water was used.

Preparation of tea leaf extract

A quantity of 10 g of finely grounded tea leaf was dissolved in 100 ml of water and boiled for 3 h. After cooling at room temperature, it was centrifuged for 30 min and filtered. The filtrate was stored at 5-10 ^oC for further experiments. An aqueous extract of green tea contains (-)-gallocatechin gallate (GCG, > 45 %), (-)-Epigallocatechin gallate (EGCG, 36 – 40 %), (-)-Epigallocatechin (EGC 0.7 – 2.3 %), and (-)-Epicatechin (EC 0.5 – 2.2 %) [31]. The structures of these major components were shown in Fig. 1. It was reported that these phenolic compounds effective at wrapping around the nanoparticles to reduce the agglomeration in the compound [32].

2.1. Synthesis

Yttrium nitrate [$Y(NO_3)_3.4H_2O$ (99.9%)] and Aluminum nitrate [$Al(NO_3)_3.9H_2O$ (99.9%)] are used as oxidizers, EGCG as a fuel and Samarium nitrate [$Sm(NO_3)_3$ (99.9%] as a dopant. The

corresponding metal nitrates and EGCG are dissolved in double distilled water in a Pyrex dish and then mixed uniformly using magnetic stirrer for ~5 min. Thereafter, the Pyrex dish is introduced in a preheated muffle furnace maintained at a temperature of $\sim 400 \pm 10$ ^{o}C. The mixture underwent dehydration with liberation of large amount of gases. Finally a product is left behind in the petri dish. The obtained product is calcined at 1000 ^{o}C for 3 h and used for characterization. The schematic diagram used for green combustion synthesis is shown in Fig. 1.

2.2. Instruments used

The phase purity and the crystallinity of the nanophosphor are examined by powder x-ray diffractometer (Shimadzu 7000) using Cuk_{α} (1.541 $\mathring{A}$) radiation with a nickel filter. The surface morphology of the product is studied by Scanning Electron Microscopy (Hitachi table top, Model TM 3000). Transmission Electron Microscopy (TEM) analysis is performed on a Hitachi H-8100 (accelerating voltage up to 200 KV, LaB_6 filament) equipped with EDS (Kevex sigma TM Quasar, USA). The FT-IR study is performed on a Perkin Elmer Spectrometer (Spectrum 1000) with KBr pellets. The UV-Vis absorption of the samples is recorded on SL 159 ELICO UV- Vis spectrometer. The photoluminescence (PL) studies are performed on a JobinYvon Spectroflourimeter Fluorolog-3 equipped with 450 W Xenon lamp as an excitation source.

2.3. Application in fingerprint development

A multitude of surface substrates are chosen for the fingerprint experiments. These included non-porous surfaces, such as aluminum foil, glass, and plastic and a porous surface of a freshly cut green leaf. The hands of fingerprint donors are sufficiently washed in soap water and air dried before making the fingerprints. Then, the cleaned fingers gently wiped the foreheads of the fingerprint donors and pressed on several different surfaces using medium pressure. To develop the resultant latent fingerprints, the $YAlO_3:Sm^{3+}$ nanophosphor is carefully applied to the surface

of the substrates with a light brushing action via a typical powder brush method. The excess powder is removed by dusting the substrate surfaces with a gentle, smooth motion until a fingerprints image is developed. The fingerprints images are photographed *in situ* with a Nikon D3100 digital camera equipped with an AF-S Nikkon 50 mm f/1.8G ED lens and a 365 nm UV light for exciting the $YAlO_3:Sm^{3+}$ nanophosphor.

3. Results and discussion

Fig.2 shows the PXRD patterns of Sm^{3+}doped $YAlO_3$ phosphor. The observed diffraction peaks are well in agreement with the standard patterns of orthorhombic (JCPDS: 70-1677) phase. Further, the sample exhibit dominant diffraction peaks of orthorhombic $YAlO_3$ along with two traces of $Y_3Al_5O_{12}$ phase. Line broadening in the XRD profile of nanocrystalline powder sample is exploited to determine the average crystallite size of the prepared nanoparticles by using Scherer's formula:

$$D = \frac{0.9\lambda}{\beta \cos\theta} \qquad \text{..... (1)}$$

Where D is the average grain size of the crystallites, λ is the incident wavelength of X-ray, θ is the Bragg's angle and β is the diffracted full width at half maximum(in radian) caused by the crystallites. The average crystallite size is found to be in the range 20-35 nm. The strain present in as-formed and Sm^{3+} doped $YAlO_3$ nanophosphor is estimated using W-H plots [33].

$$\beta \cos\theta = \frac{0.9\lambda}{D} + 4\varepsilon \sin\theta \qquad \text{..... (2)}$$

where ε is the strain associated with the nanoparticles. Eq. (2) represents a straight line between $4\sin\theta$ (X-axis) and $\beta\cos\theta$ (Y-axis). The slope of the line gives the strain (ε) and the intercept (0.9λ/D) of this line on the Y- axis gives the strain size (D) (Fig.3). From Table.1 it could be observed that the grain size determined from W-H plots are slightly higher than those calculated

using Scherer's formula. The small disparity in these values might be due to the fact that strain component is assumed to be zero and the observed broadening of diffraction peak is considered as a result of reducing grain size in Scherer's formula.

The acceptable percentage difference in ionic radii between doped and substituted ions should not exceed 30%. The calculations of the radius percentage difference (D_r) between the doped ions (Sm^{3+}) and substituted ions (Y^{3+}) in $YAlO_3:Sm^{3+}$ is estimated using the following relation.

$$D_r = \frac{R_m(CN) - R_d(CN)}{R_m(CN)} \quad \text{---------- (3)}$$

Where CN is Co-ordination number, $R_m(CN)$ is radius of host cations and $R_d(CN)$ is radius of dopant ion and it is found to be 5.3 %. Thus, it clearly indicates that the Sm^{3+}ionic radius (r=1.132 Å,CN=9) is very close to that of Y^{3+}(r =1.075 Å,CN=9), making it unlikely that Sm^{3+} ions would substitute with Y^{3+} in the $YAlO_3$ host. Hence, it is believed that the Y^{3+}sites are replaced by Sm^{3+}in the lattice [34].

Fig.4 (A-C) shows the surface morphology of Sm^{3+} (0.5–11mol %) doped $YAlO_3$ nanophosphors is studied using SEM. It is evident from images that, the powders show almost spherical shape with diameter of ~ 3 μm. The TEM image (Fig.4D) further confirms that average crystallites size is in the range 20 – 40 nm, which is very close to the value obtained by the PXRD measurements and further endorses the nano regime. The TEM image further classifies that the $YAlO_3:Sm^{3+}$ particles are spherical in shape.

Fig. 5 shows the AFM images of the samples in Z- axis scan range of 1.86 μm and 3-D axis scan of 1.86 μm x 1.86 μm x 22.4 nm along X, Y and Z- axis respectively. The images confirms the nano superstructures with almost oriented in a particular angle of about 30 – 42 ° range from Z-axis. The surface roughness of the samples were ~ 40 nm.

The UV–Vis absorption spectra for Sm^{3+} doped $YAlO_3$ nanophosphors measured in the wavelength range 200 - 600 nm is shown in Inset of Fig. 6. The maximum absorption peak (~276 nm) shifts towards higher wavelength side due to transition between valence band and conduction band. The weak absorption peak (~247 nm) in the UV–visible region is attributed to the impurities/surface traps/defects [35]. The direct energy band gap (E_g) is estimated for Sm^{3+} doped $YAlO_3$ nanophosphor from UV–Vis spectra (Fig. 6) by using Wood and Tauc relation [36]. The E_g values are found to be in the range 5.45 - 5.59 eV and well matched to those found in literature [37].

Fig. 7 shows the FTIR spectra of $YAlO_3:Sm^{3+}$ (0.5 – 11 mol %) phosphors. The band at 3438 cm^{-1} is well assigned to vibration mode of chemically bonded hydroxyl groups and this band decreases as the dopant concentration increases. The band at 1468 cm^{-1} is attributed to the bending mode of H–O–H vibrations [38]. The sharp peak at 701 cm^{-1} is due to the stretching mode of Al–O in octahedral coordination state (AlO_6 octahedral).

The inset of Fig. 8 shows the excitation spectrum of $YAlO_3:Sm^{3+}$ (11 mol %) monitored at 601 nm. The spectrum displayed four f–f transitions, which could be ascribed to the transitions 317, 333, 368 and 440 nm of Sm^{3+} ions. Charge transfer band of Sm^{3+}–O^{2-} interaction or host absorption band is not detected. This is due to weak interaction of Sm^{3+} ions with the host lattice. Therefore energy transfer doesn't occur between Sm^{3+} and host.

The PL emission spectra (Fig.8) of the Sm^{3+} (0.5-11 mol %) doped $YAlO_3$ nanophosphor is recorded upon excited at 368 nm. When Sm^{3+} ions excited to the typical and intense $^6H_{5/2} \rightarrow {}^6P_{3/2}$ level, the excited ions finally relaxed at the $^4G_{5/2}$ level by the nonradioactive relaxation process. Several energy levels appeared between $^6P_{3/2}$ and $^4G_{5/2}$ with smaller energy

differences, which stimulate the non-radioactive process, resulting in the population of $^4G_{5/2}$ level, and facilitate the presence of Sm^{3+} emission peaks. The emission spectra exhibited dominant peaks at 564, 601 and 647 nm are due to the f-f forbidden transitions of the 4f electrons of Sm^{3+} corresponding to $^4G_{5/2}\rightarrow{}^6H_{5/2}$, $^4G_{5/2}\rightarrow{}^6H_{7/2}$ and $^4G_{5/2}\rightarrow{}^6H_{9/2}$ respectively [39]. Among them, the intense emission peak is observed at 601 nm due to ($^4G_{5/2}\rightarrow{}^6H_{7/2}$) transition. The results are in good agreement with the previous reports [40-42]. It is well known that the magnetic dipole (MD) transitions obey the selection rule $\Delta J=0$ and ±1 (J: is the angular momentum) and electric dipole (ED) transitions obey the selection rule $\Delta J\leq6$ unless J or $J^1=0$ when $\Delta J=2,4,6$ [43]. In case of Sm^{3+} ions, the $^4G_{5/2}\rightarrow{}^6H_{5/2}$ ($\Delta J=0$) at 564 nm and $^4G_{5/2}\rightarrow{}^6H_{7/2}$ ($\Delta J = 1$) at 601 nm belong to MD transitions, while the $^4G_{5/2}\rightarrow{}^6H_{9/2}$ ($\Delta J=2$) at 647 nm is related to ED transition. In order to understand the symmetry of the local environment around the trivalent $4f^5$ ions, the intensity ratio of ED to MD is explored as shown in Fig.9. The ratio is close being connected to asymmetry nature. Moreover, the symmetry environment of luminescent site decreases, the intensity of hyper sensitive transition $^4G_{5/2}\rightarrow{}^6H_{9/2}$ increases [44]. It is well known that the luminescence performance of the prepared samples are depends on the concentration of the activator ions. Thus, it is necessary to identify the optimal concentration for better results. It is observed from Fig. 10, that the emission intensities are gradually decreasing from 1 mol% Sm^{3+}, due to concentration quenching. The concentration quenching might be owing to the cross –relaxation process between the neighboring Sm^{3+} ions from the two different crystallographic sites by reducing the distance with higher doping concentration. Once the distance is shorter than the critical value, the energy may probably transferred from one activator to another one and eventually reaches the quenching sites, rather than being released from individual activators in the form of light emission. The energy gap between the $^4G_{5/2}$and $^6F_{9/2}$ is

close to that of $^6H_{5/2}$ and $^6F_{9/2}$ levels. Therefore, if the Sm^{3+} ions concentration reaches the optimum condition, the higher energy level emission is easily quenched by means of lower energy level emission [45].

At higher doping concentration, the number of Sm^{3+} ions increases and hence distance among the activator ions decreases which intern leads to the non- radioactive energy transfer among Sm^{3+} ions giving rise to the decrease in the emission intensity [46]. In this context, the critical distance (R_c) can be estimated from the following equation [47].

$$R_c \approx 2\left(\frac{3V}{4\Pi X_c N}\right)^{\frac{1}{3}} \quad \text{---------- (4)}$$

where V is the volume of the unit cell, X_c is the critical concentration and *N* is the number of cationic sites in the unit cell. In the present work, V is 204.10Å^3, X_c is about 0.01and N is4, resulting in the critical distance of~21.36Å. Generally, the resonant energy-transfer mechanism is ruled by exchange and multi polar interactions. Previous studies have indicated that the critical distance between the sensitizer and the activator should be shorter than 5Å for the energy transfer results from exchange interaction [48], which is far less than that of the above calculated result of Sm^{3+} doped $YAlO_3$. This finding suggests that the energy transfer among Sm^{3+} ions in $YAlO_3$:Sm^{3+} (0.5-11 mol %) phosphor does not occur in this case. Hence, the process of energy transfer should be electric multipole interaction. VanUitert [49] reported that the intensity of multi- polar interaction can be determined based on the change in the emission intensity from the emitting level that has multipolar interaction. The emission intensity (I) per activator ion follows the equation:

$$\frac{I}{X} = K\left[1+\beta(\chi)^{\frac{Q}{3}}\right]^{-1} \quad \text{---------- (5)}$$

Where χ is the activator concentration, Q is a constant of multi- polar interaction and equals 6, 8 or 10 for dipole–dipole, dipole– quadrupole or quadrupole–quadrupole interaction respectively, and K and β are constants under the same excitation condition for the given host crystal. Eq. (5) can be approximately reduced to Eqs. (6) for $\beta\chi^{\frac{Q}{3}} \rangle\rangle 1$ as follows:

$$Log\frac{I}{X} = A - \frac{Q}{3}\log\chi\left(A = \log k - \log\beta\right) \quad \text{---------- (6)}$$

The curve of log I/x v/s log x in $YAlO_3:Sm^{3+}$ phosphor is shown in Fig. 11. The figure clearly indicates that the relation between log I/x and log x is approximately linear and the slope is about -0.917. The Q value calculated based on the linear fitting using Eq. (6) is 6.4, which is close to 6.This indicates that the dipole–dipole interaction is the major mechanism for the concentration quenching of the fluorescence emission of Sm^{3+} ions in $YAlO_3$ phosphor.

The Judd–Ofelt analysis of the emission spectrum is a powerful tool and has been extensively used to analyze the radiative transitions of rare-earth ions in several host materials [50, 51]. By means of the calculation of the J–O intensity parameters Ω_t (t=2, 4) from the emission spectra, the spontaneous emission probability, asymmetric ratio and radiative lifetime of excited manifold can be estimated. For most of the transitions, the probability for magnetic dipole transitions is much smaller than those for the forced electric dipole transitions $A_{md}\left[J \to J'\right] \langle A_{ed}\left[J \to J'\right]$. However, in certain cases, they may significantly contribute to the total $J \to J'$ radiative transition probability. For the slight contributions to the line strengths of Sm^{3+} ions, the magnetic dipole transitions are not taken into account in the J–O calculations, and only the electric dipole transitions are considered. The excitation line strength for an ED transition can be expressed in terms of J–O intensity parameters $\Omega_{2,4}$ by

$$S_{calc}^{ed}(J \to J') = \sum_{t=2,4} \Omega_t \left| \left\langle \varphi^J \left\| U^t \right\| \varphi^{J'} \right\rangle \right|^2 \qquad \text{---------- (7)}$$

where the matrix elements $\left\langle \left\| U^t \right\| \right\rangle$ are doubly reduced unit tensor operator[52] of rank t calculated in the intermediate coupling approximation and are independent of the crystal host. The parameters Ω_2 and Ω_4 exhibit the influence of the host on the transition probabilities since they contain the crystal-field parameters, inter configurational radial integrals, and the interaction between the central ion and intermediate environment.

The measured line strengths (S_{ed}^{meas}) were calculated from the emission spectrum by:

$$S_{meas}^{ed}(J \to J') = \frac{3ch(2J+1)}{8\Pi^3 \bar{\lambda} e^2 N_0} \frac{9n}{(n^2+2)^2} \Gamma_{emis} \qquad \text{---------- (8)}$$

where J (J'): the angular momentum quantum number of the initial (final) state of rare earth ion, n: the refractive index of the sample, $\bar{\lambda}$: the mean wavelength of the excitation band, N_0: rare earth ion concentration and Γ_{emis} : the integrated emission intensity for each band from the initial state to the final state which is similar to the integrated absorbance for the absorption spectrum [53]. The factor $9n/(n^2+2)^2$ in eqn. (8) is the local field correction for the ion in the dielectric host medium. The measured line strengths were then used to obtain the J–O parameters Ω_2 and Ω_4 by solving a set of n number of equations for the corresponding transitions between J and J'. A least squares fit method is used for eqn. (7) and (8) to get a good fit between the calculated and measured line strengths as well as to obtain J–O intensity parameters (Ω_t).

The Judd–Ofelt parameters Ω_2 and Ω_4 are obtained using least-squares fitting approach between the S_{meas} and the S_{cal}. The J–O parameters, for various concentrations of Sm^{3+} doped $YAlO_3$ nanophosphors are tabulated in Table 2. The experimental value of Ω_2 is most sensitive to the ligand environment which can be clearly observed by the change of its value with

concentration of Sm^{3+} ions. According to previous studies, the Ω_2 parameter increases with the asymmetry of the local structure and the degree of covalency of the lanthanide-ligand bonds, whereas the Ω_4 parameter decreases with the degree of covalency. Large values for Ω_4 can be expected for organic ligands, because of low rigidity of the host [54, 55].

The radiative transition probabilities and radiative lifetime were important dynamic parameters for trivalent rare earth ions. The radiative lifetime τ_{rad} for an excited state (J) was calculated by

$$\tau_{rad} = \frac{1}{\sum A(J - J')} \qquad \text{---------- (9)}$$

where the sum taken over all final lower-lying states J'. The radiative decay rate for the transitions determined by using Eq. (9) was given in Table 2.

$$A(J - J') = \frac{64\prod^4 e^2}{3h(2J+1)\lambda^3}\frac{n(n^2+2)^2}{9}S_{calc}(J - J') \qquad \text{---------- } \textit{(10)}$$

The estimated parameters for the Sm^{3+} ion in $YAlO_3$ host are listed in Table 2.

The Commission International De I-Eclairage (CIE) chromaticity co-ordinates of $YAlO_3$:Sm^{3+} (1 mol %) phosphors are calculated for the optimized Sm^{3+} ion concentration (Fig. 12). The CIE coordinates (x = 0.296, y = 0.237) are determined to be located in the pure white region. The obtained CIE coordinates from the PL studies is close vicinity to that of the ideal white light. This white color emitting phosphor may be useful in the production of artificial white light to be similar to those of natural white light. The correlated color temperature (CCT) can be estimated by Planckian locus, which is only a small portion of the (x, y) chromaticity diagram. If the coordinates of a light source do not fall on the Planckian locus, the correlated color temperature (CCT) is used to define the color temperature of a light source. CCT is

calculated by transforming the (x, y) coordinates of the light source to (U_0, V_0) by using following equations, and by determining the temperature of the closest point of the Planckian locus to the light source on the (U_0,V_0) uniform chromaticity diagram (Fig. 13) [56, 57].

$$U' = \frac{4x}{-2x+12y+3} \quad \text{---------- (11)}$$

$$V' = \frac{9y}{-2x+12y+3} \quad \text{---------- (12)}$$

CCT is found to be 11900 K using $U^1 = 0.2254$ and $V^1 = 0.4064$.

3.1 Fingerprint detection using $YAlO_3$: Sm^{3+} (1 mol %) nano-phosphor

All the finger marks were collected from the same donor. Initially, hands were washed thoroughly with soap solution. The fingers were then gently wiped across the forehead. Finally, the fingers were pressed on the surfaces of different substrates at room temperature to obtain latent finger marks. The main purpose of experiment is the production of $YAlO_3$:Sm^{3+} nano-phosphor with good photoluminescence property, which could make latent fingerprints visible under long UV illumination. The schematic view for the fingerprint development is shown in Fig.14. The optimized $YAlO_3$:Sm^{3+} (1 mol %) nanophosphor show exceptional UV radiation-dependent photoluminescence. The obtained $YAlO_3$:Sm^{3+} (1 mol %) nanophosphor overcome the tendency to oxidize in air, which may result in weakening of photoluminescence. Thus, it is possible that the obtained $YAlO_3$:Sm^{3+} (1 mol %) nanophosphor may be used as a series of alternative phosphorescent labeling markers for enhanced latent fingerprint detection on a variety of object surfaces in forensic science for individual identification.

Fig. 15 shows the photographs of latent fingerprints detected by using $YAlO_3$:Sm^{3+} (1 mol %) nanophosphor phosphorescent labeling markers on a variety of surfaces like aluminum foil, glass, and plastic. Owing to the nanosized phosphor they show good adhesion for finger

mark ridges. It can be seen clearly from Fig. 15 that the fingerprint is well-defined in terms of finger ridge details without background staining, resulting in good contrast for enhanced detection and also demonstrating that our developing method is versatile and can be applied to detect fingerprints on virtually all smooth objects.

The porous surface of freshly cut green leaves represents one of the difficult, but frequently encountered, substrates for recovering latent fingerprints. Our $YAlO_3:Sm^{3+}$ (1 mol %) nanophosphor appeared to be able to identify the fingerprints with reasonable details (Fig. 16 a-d).

Our results show that $YAlO_3:Sm^{3+}$ (1 mol %) nanophosphor can image whole fingerprint with high efficiency (because the whole procedure is fast and could be finished in approximately 30 s for trained investigators) and high sensitivity (because sweat pores can be observed owing to the small particle size). Specifically, the whole procedure is simple and rapid; an investigator only needs to apply pre-synthesized $YAlO_3:Sm^{3+}$ (1 mol %) nanophosphor onto the finger marks, immediately followed by imaging the fingerprint marks under a 365 nm UV light source. Further finger marks also contain bio molecules such as DNA, which serves as an additional marker for identifying an individual. The DNA collected from finger marks after finger mark development could be analyzed and used to identify individuals. Based on the detailed results, it is likely to confirm that with this fluorescent material applied in the development of finger marks establishes the possibility to distinguish the main features (shown in Fig 17) of a finger mark in various surfaces in a database, in terms of type and shape.

Further, the other materials which are used in the literature are generally nanoparticles of gold, amphiphilic silica, $ZnO\text{-}SiO_2$ (40-50 percent zinc and 10-20 percent silicon.), carbogenic based upconversion lysozyme-binding functionalized nanoparticles. Compared to these

materials our material with optimized $YAlO_3:Sm^{3+}$ nanophosphors applied to latent fingerprints produced clear fluorescent impressions when illuminated with 365 nm UV light.

4. Conclusions

A simple and inexpensive combustion method is used to prepare Sm^{3+} doped $YAlO_3$ perovskite within a few minutes at low temperature (400 ± 10 ^oC). The average crystallite size is found to be in the range 20 - 35 nm, which is in good agreement with the W - H plots. The crystallites are in spherical in shape. The UV–Vis absorption spectra display a maximum absorption peak at ~274 nm. The energy gap (E_g) values are found to be in the range 5.45 - 5.59 eV. The PL emission peaks at 564, 601 and 647 nm are attributed to f-f forbidden transition of Sm^{3+} ions in $YAlO_3$: Sm^{3+} phosphor. The CIE coordinate values for Sm^{3+} doped $YAlO_3$ nanophosphor are located within the white region and CCT for optimized Sm^{3+}:$YAlO_3$ phosphor is found to be 11900 K. The present work shows that $YAlO_3$: Sm^{3+} phosphor is a versatile fluorescent label for the facile detection of fingerprint marks on virtually any material, enabling their practical applications in Forensic Sciences as well as display devices. The $YAlO_3:Sm^{3+}$ nanoparticles may be used as alternative fluorescent markers for enhanced latent finger detection on a variety of objects in criminal science for individual identification. The optimized $YAlO_3:Sm^{3+}$ nanophosphors applied to latent fingerprints produced clear fluorescent impressions when illuminated with 365 nm UV light.

Acknowledgements

Author HBP thanks VGST, Government of Karnataka, India, (No. VGST/P-3/SMYSR/GRD-302/2013-14) for its help in carrying out this research work .

References

[1]. M. Saif, Magdy Shebl, A.I. Nabeel, R. Shokry, H. Hafez, A. Mbarek, K. Damak, R. Maalej, M.S.A. Abdel-Mottale, Novel non-toxic and red luminescent sensor based on Eu^{3+}:$Y_2Ti_2O_7/SiO_2$ nano-powder for latent fingerprint detection, Sensors and Actuators B 220 (2015) 162–170.

[2]. C.H. Huang, P.J. Wu, J.F. Lee, T.M. Chen, "(Ca, Mg, Sr)$_9$Y(PO$_4$)$_7$:Eu^{2+}, Mn^{2+}: Phosphors for white-light near-UV LEDs through crystal field tuning and energy transfer", J. Mater. Chem. 21 (2011) 10489-10495.

[3]. S. Vaidyanathan, D.Y. Joen, "A Novel Narrow Band Red-Emitting Phosphor for White Light Emitting Diodes", Int. J. Appl. Ceram. Technol. 6 (2009) 453-458.

[4]. J.R. DiMaio, B. Kokuoz, J. Ballato, "White light emissions through down-conversion of rare-earth doped LaF_3 nanoparticles", Opt. Express 14 (2006) 11412-11417.

[5]. S. Yang, C. Stoffers, F. Zhang, S. M. Jacobsen, B. K. Wagner, and C. J. Summers, "Green phosphor for low-voltage cathodoluminescent applications: $SrGa_2S_4$:Eu^{2+}", Appl. Phys. Lett.72, (1998) 158 – 160.

[6]. P.K Jisha, R. Naik, S.C. Prashantha, H. Nagabhushana, S.C. Sharma, H.P. Nagaswarupa, H.B. Premkumar, "Facile combustion synthesized orthorhombic $GdAlO_3$:Eu^{3+} nanophosphors: Structural and photoluminescence properties for WLEDs", J. Lumin. 163 (2015) 47–54.

[7]. Ramachandra Naik, S.C. Prashantha, H. Nagabhushana, H.P. Nagaswarupa, K.S. Anantharaju, S.C. Sharma, B.M. Nagabhushana, H.B. Premkumar, K.M. Girish, "$Mg_2SiO_4:Tb^{3+}$ nanophosphor: Auto ignition route and near UV excited photoluminescence properties for WLEDs", J. Alloy Compd. 617 (2014) 69-75.

[8]. P. Guo, F. Zhao, G. Li, F. Liao, S. Tian, and X. Jing," Novel phosphors of Eu^{3+}, Tb^{3+} or Bi^{3+} activated Gd_2GeO_5",J. Lumin. 105 (2003) 61-67

[9]. A. Vecht, C. Gibbons, D. Davies, X. Jing, P. Marsh, T. Reland, J. Silver, A. Nowport, and D. Barber, "Engineering phosphors for field emission displays", *J. Vac. Sci. Technol. B*, 17(1999) 750 – 757.

[10]. Xiaoming Liu, Jianping Zou, and Jun Lin, "Nanocrystalline $LaAlO_3: Sm^{3+}$ as a Promising Yellow Phosphor for Field Emission Displays" J. Elec. chem. Soc.156 (2) (2009) 43 – 47.

[11]. Y. Quanmao, L. Yufeng, W. Shan, L. Xingdong, H. Xinyang, L. Xiaoxia, "Luminescent properties of $Ca_2SiO_4:Eu^{3+}$ red phosphor for trichromatic white light emitting diodes", J. Rare Earth 26 (2008) 783-786.

[12]. Qilin Dai, M. E. Foley, C. J. Breshike, A. Lita, G. F. Strouse, "Ligand-Passivated $Eu:Y_2O_3$ Nanocrystals as a Phosphor for White Light Emitting Diodes", J. Am. Chem. Soc. 133 (2011) 15475–15486.

[13]. W. Hao, Z. Xinmin, G. Chongfeng, X. Jian, W. Mingmei, S. Qiang, "Three-Band White Light From InGaN-Based Blue LED Chip Pre coated With Green/Red Phosphors" IEEE Photon. Technol. Lett.17 (2005) 1160 – 1162.

[14]. J.K. Park, C.H. Kim, S.H. Park, H.D. Park, S.Y. Choi, "Application of strontium silicate yellow phosphor for white light-emitting diodes",Appl. Phys. Lett. 84 (2004) 1647 - 1649.

[15]. J.H. Oh, K.-H. Lee, H.C. Yoon, H. Yang, Y.R. Do, "Color-by-blue display using blue quantum dot light-emitting diodes and green/red color converting phosphors" Opt. Express, 22 (2014) A511-A520.

[16]. Y. Shimomura, T. Honma, M. Shigeiwa, T. Akai, K. Okamoto, N. Kijima, " Photoluminescence and Crystal Structure of Green-Emitting $Ca_3Sc_2Si_3O_{12}:Ce^{3+}$ Phosphor for White Light Emitting Diodes Sensors and Displays: Principles, Materials, and Processing", J. Electrochem. Soc. 154 (2007) J35-J38.

[17]. K.L. Frindell, M.H. Bartl, A. Popitsch, G.D. Stucky, Angew. "Sensitized Luminescence of Trivalent Europium by Three-Dimensionally Arranged Anatase Nanocrystals in Meso structured Titania Thin Films" Chem. Int. Ed. 41 (2002) 959–962.

[18]. A. Conde-Gallardo, M. Garcia-Rocha, I. Hernandez-Calderon, R. Palomino Merino, "Photoluminescence properties of the Eu^{3+} activator ion in the TiO_2 host matrix" Appl. Phys. Lett. 78 (2001) 3436–3438.

[19]. M. Medraj, R. Hammond, M.A. Parvez, R.A.L. Drew, W.T. Thompson, "High temperature neutron diffraction study of the Al_2O_3–Y_2O_3 system", J. Eur. Ceram. Soc. 26 (2006) 3515–3524.

[20]. I. Warshaw, R. Roy, "Stable and Metastable Equilibria in the Systems Y_2O_2-Al_2O_3, and Gd_2O_3-Fe_2O_3", J. Am. Ceram. Soc. 42 (1959) 434–438.

[21]. S. Mathur, H. Shen, R. Rapalaviciute, A. Kareiva, N. Donia, "Kinetically controlled synthesis of metastable $YAlO_3$ through molecular level design", J. Mater. Chem. 14 (2004) 3259–3265.

[22]. J.F. Carvalho, F.S. De Vicente, S. Pairis, P. Odier, A.C. Hernandes, A. Ibanez, "Synthesis of YAP nanopowder by a soft chemistry route", J. Eur. Ceram. Soc. 29 (2009) 2511–2515.

[23]. S. Wang, X. Wang, H. Rhee, S. Meister, H.J. Eichler, J. Chen,"Pulsed Nd:YAP laser at 1432 nm pumped with high power laser diode**"**, Opt. Commun. 283(2010) 2881-2884.

[24]. G.C. Kim, H.L. Park, T.W. Kim, "Emission color tuning from blue to green through cross-relaxation in heavily Tb^{3+}-doped $YAlO_3$", Mater. Res. Bull. 36 (2001) 1603-1608.

[25]. W.C. Lv, X.H. Ma, H. Zhou, G.T. Chen, J.F. Li, Z.J. Zhu, Z.Y. You, C.Y. Tu,"White Up-Conversion Luminescence in Rare-Earth-Ion-Doped $YAlO_3$ Nanocrystals", J. Phys. Chem. C 112 (2008) 15071-15074.

[26]. J. Marchal, T. John, R. Baranwal, T. Hinklin, R.R. Laine, "Yttrium Aluminum Garnet Nanopowders Produced by Liquid-Feed Flame Spray Pyrolysis (LF-FSP) Metalloorganic Precursors", Chem. Mater. 16 (2004) 822-831.

[27]. Ramachandra Naik, S.C. Prashantha, H. Nagabhushana, S.C. Sharma, H.P. Nagaswarupa, K.S. Anantharaju, B.M. Nagabhushana, H.B. Premkumar, K.M. Girish, "A single phase, red emissive $Mg_2SiO_4:Sm^{3+}$ nanophosphor prepared via rapid propellant combustion route", Spectr Acta Part A: Molec Biom Spectr. 140 (2015) 516–523.

[28]. M. Puchalska, E. Zych, "Theeffect of charge compensation by means of Na^+ ions on the luminescence behavior of Sm^{3+} - doped $CaAl_4O_7$ Phosphor" J. Lumin. 132 (2012) 826-831.

[29]. Huajuan Deng, Ze Zhao, Jing Wang, ZhoufeiHei, Mengxue Li, Hyeon Mi Noh, Jung Hyun Jeong, Ruijin Yu, "Photoluminescence properties of a new orange–red emitting Sm^{3+}-doped $Y_2Mo_4O_{15}$ phosphor", journal of Solid State Chemistry, 228(2015) 110-116.

[30]. G. Ramakrishna, H. Nagabhushana, S.C. Prashantha, S.C. Sharma, B.M. Nagabhushana, "Role of flux on morphology and luminescence properties of Sm^{3+} doped Y_2SiO_5 nanopowders for WLEDs", Spectr Acta Part A: Molec Biom Spectr. 136 (2015) 356-365.

[31] Mohanpuria P, Rana N K and Yadav S K 2008 J. Nanopart. Res. 10 507.

[32] Honary S, Barabadi H, Gharaei-Fathabad E and Naghibi F 2012 Digest J. Nanomater. Biostruct. 7 999

[33]. G.K. Williamson, W.H. Hall, "X-ray line broadening from filed aluminum and wolfram", Acta Metall. 1 (1953) 22-31.

[34]. D. Chikte (Awade), S.K. Omanwar, S.V. Moharil, "Luminescence properties of red emitting phosphor $NaSrBO_3$:Eu^{3+} prepared with novel combustion synthesis method", J. Lumin. 142 (2013) 180–183.

[35]. L.K. Pan, Q. Sun Chang, C.M. Li, "Elucidating Si−Si Dimmer Vibration from the Size-Dependent Raman Shift of Nanosolid Si", J. Phys. Chem. B 108 (2004) 3404–3406.

[36]. J.Tauc, F. Abeles (Ed.), Optical Properties of Solids, North-Holland,Amsterdam,1970.

[37]. H.B. Premkumar, H. Nagabhushana, S.C. Sharma, S.C. Prashantha, H.P. Nagaswarupa, B.M. Nagabhushana, R.P.S. Chakradhar, "Structural, photo and thermoluminescence studies of Eu^{3+} doped orthorhombic $YAlO_3$ nanophosphors", J. Alloy Compd., 601 (2014) 75 – 84

[38]. H.B. Premkumar , B.S. Ravikumar , D.V. Sunitha , H. Nagabhushana , S.C. Sharma , M.B. Savitha ,S. Mohandas Bhat , B.M. Nagabhushana , R.P.S. Chakradhar, "Investigation of structural and luminescence properties of Ho^{3+} doped $YAlO_3$ nanophosphors synthesized through solution combustion route", Spectrochim. Acta, Part A 115 (2013) 234–243.

[39]. Li Changmin, Yang Dianlai, Zhang Yingying, Wang Zhiqiang, "Photoluminescence Characterization of Sm^{3+} -Doped Fluoroborate Ceramics",J. Rare Earths,Vol.25, (2007) 143-146.

[40]. V.Kiisk, I.Sildos, S.Lange, V.Reedo, T.Tatte, M.Kirm, J.Aarik, "Photoluminescence characterization of pure and Sm^{3+}-doped thin metaloxide films", Appl.Surf.Sci.247 (2005) 412–417.

[41]. Z.Assefa, R.G.Haire, P.E.Raison, "Photoluminescence and Raman studies of Sm^{3+} and Nd^{3+} ions in zirconia matrices: example of energy transfer and host–guest interactions", Spectrochim.Acta,PartA60 (2004)89–95.

[42]. L.Hu, H.Song, G.Pan, B.Yan, R.Qin, Q.Dai, L.Fan, S.Li, X.Bai,"Photoluminescence properties of samarium-doped TiO_2 semiconductor nanocrystalline powders", J.Lumin.127 (2007) 371–376.

[43]. S. Shionoya, W.M. Yen, H.Yamamoto, Phosphor Handbook, Taylor and Francis,2010

[44]. Jinsheng Liao, Liangbin Liu, Hangying You, Haiping Huang, Weixiong You, "Hydrothermal preparation and luminescence property of $MWO_4:Sm^{3+}$ (M = Ca, Sr, Ba) red phosphors", Optik 123 (2012) 901-905.

[45]. G Seeta Rama Raju, Jae Su Yu, "Novel orange and reddish-orange color emitting $BaGd_2O_4:Sm^{3+}$ nanophosphors by solvo thermal reaction for LED and FED applications", Spectrochim. Acta, Part A 124 (2014) 383-388.

[46]. Hom Nath Luitel, Takanori Watari, Rumi Chand, Toshio Torikai, Mitsunori Yada, "Photoluminescence properties of a novel orange red emitting $Sr_4Al_{14}O_{25}:Sm^{3+}$ phosphor and PL enhancement by Bi^{3+} co-doping", Opt. Mater. 34 (2012) 1375-1380.

[47]. L.G. Van Uitert, "Characterization of Energy Transfer Interactions between Rare Earth Ions", J. Electrochem. Soc.114 (1967) 1048-1053.

[48]. B.R. Judd, "Optical absorption intensities of rare-earth ions", Phys Rev. 127 (1962)750 761.

[49]. G.S. Ofelt, "Intensities of crystal spectra of rare-earth ions", J. Chem Phys. 37 (1962) 511-520.

[50]. O.L. Malta, M.A. Couto dos Santos, L.C. Thompson, N.K. Ito, "Intensity parameters of4f—4f transitions in the Eu (dipivaloylmethanate)$_3$ 1,10-phenanthroline complex", J.Lumin. 69 (1996) 77-84.

[51]. B.R. Judd, "Optical absorption intensities of rare-earth ions", Phys Rev. 127 (1962)750-761.

[52]. G.S. Ofelt, "Intensities of crystal spectra of rare-earth ions", J. Chem Phys. 37 (1962) 511-520.

[53]. C. K. Jayasankar , E. Rukmini, "Optical properties of Sm 3+ ions in zinc and alkali zinc borosulphate glasses", Opt. Mater., 8 (1997) 193.

[54]. W. Luo, J. Liao, R. Li and X. Chen, "Determination of Judd–Ofelt intensity parameters from the excitation spectra for rare-earth doped luminescent materials", Phys. Chem. Chem. Phys., 12 (2010) 3276.

[55]. Z. Duan, "Spectroscopic properties and Judd-Ofelt theory analysis of Dy^{3+} doped oxyfluoride silicate glass", J. Appl phys. 101 (2007) 043110.

[56]. B. Judd, J. Deane, "Estimation of Chromaticity Differences and Nearest Color Temperature on the Standard 1931 ICI Colorimetric Coordinate System", Opt. Soc. Am. 26 (1936) 421–426.

[57].J. Schanda, M. Danyi, "Correlated Color-Temperature Calculations in the CIE 1976 Chromaticity Diagram",Color Res. Appl. 2 (1977) (1976) 161–163.

[58]. W. Huang, X. Li, H. Wang, X. Xu, H. Liu, G. Wang, "Synthesis of Amphiphilic silica nanoparticles for latent fingerprint detection", Anal. Lett., 48 (2015)1524 – 1535.

[59] D. Fernandes, M. J. Krysmann, A. Kelarakis, "Carbon dot based nanopowders and their application for fingerprint recovery", Chem. Commun. 51 (2015) 4902 – 4905.

[60]. J. Wang, t. Wei, X. Li, B. Zhang, J. Wang, C. Huang, Q. Yuan, "Near-infrared-light-mediated imaging of latent fingerprints based on molecular recognition", Angew. Chem. INt. Edu. Engl. 53 (2014) 1616 – 1620.

Table captions:

Table 1: Estimated crystallite and strain values of $YAlO_3:Sm^{3+}$ nanophosphor.

Table 2: Judd-Ofelt intensity parameters (Ω_2, Ω_4), Emission peak wavelengths ($\lambda_p$in nm), radiative transition probability (A_T), calculated radiative (τ_{rad}) lifetime and asymmetric ratio of $YAlO_3$: Sm^{3+} compounds (λ_{ex} = 368 nm).

Figure captions:

Fig. 1 .Flowchart for the preparation of $YAlO_3$: Sm^{3+} nanophosphor

Fig.2. PXRD patterns of (0.5–11 mol %) Sm^{3+} doped $YAlO_3$ nanophosphor.

Fig.3. W–H plots of $YAlO_3:Sm^{3+}$ (0.5–11 mol %).

Fig. 4(A–D).SEM micrographs of $YAlO_3:Sm^{3+}$ (1, 3, 7 and11 mol %) nanophosphor, (E and F) TEM and SAED image of $YAlO_3:Sm^{3+}$ (5 mol %).

Fig.5. AFM images of 1 mol% Sm^{3+} doped $YAlO_3$ nanophosphor

Fig.6.Energy band gaps of (0.5–11 mol %) Sm^{3+} doped $YAlO_3$ nanophosphors.

(Inset: Uv–Vis absorption spectra of (0.5-11 mol %) Sm^{3+}doped$YAlO_3$)

Fig.7. FTIR spectra of $YAlO_3:Sm^{3+}$ (0.5-11 mol %) nanophosphors.

Fig.8. PL spectra of $YAlO_3:Sm^{3+}$(0.5–11mol %) nanophosphors recorded at RT.

(Inset Excitation spectra of $YAlO_3:Sm^{3+}$(11 mol %) at $\lambda_{emi} = 601$ nm)

Fig.9. Variation of asymmetric ratio with Sm^{3+}concentration in $YAlO_3$ nanophosphors

Fig.10. Effect of Sm^{3+}concentration on the 601 nm emission peaks in $YAlO_3$ nanophosphors

Fig.11. Relation between log(x) and log (I/x) in $YAlO_3:Sm^{3+}$(0.5–11mol %) nanophosphors.

Fig.12. CIE diagram of $YAlO_3:Sm^{3+}$ (1mol %) nanophosphor.

Fig.13. CCT diagram of $YAlO_3$: Sm^{3+}(1 mol%) nanophosphor.

Fig.14. Illustration of the development of latent fingermarks using a $YAlO_3$: Sm^{3+} (1 mol %) nanophosphor dusting process. A fingermark was printed on a glass. Then, $YAlO_3:Sm^{3+}$ (1 mol %) nanophosphor powder was deposited onto the substrate to stain the fingermark.

A 365 nm UV light was then used to irradiate the fingermark, leading to the excitation of $YAlO_3$: Sm^{3+} (1 mol %) nanophosphor to emit white light and consequently revealing the fingermark with high sensitivity and contrast.

Fig.15. Latent fingermarks stained by $YAlO_3$:Sm^{3+} (1 mol %) nanophosphor and detected on the surface of various substrates after 365 nm UV light irradiation: (a) aluminum foils (b) Glass (c) transparent plastic sheet (d) stainless steel (e) freshly cut leaf

Fig.16. Latent fingermarks stained by $YAlO_3$:Sm^{3+} (1 mol %) nanophosphor for analysis of correspondences.

Fig. 17. Latent fingermarks aged on the surface of glass for various periods of time, stained by YAlO3:Sm^{3+} (1 mol %) and finally detected by 365 nm UV light irradiation (a) 1 day (b) 5 days (c) 10 days (d) 30 days.

Table 1: Estimated crystallite and strain values of $YAlO_3:Sm^{3+}$ nanophosphor.

$YAlO_3:Sm^{3+}$	**Crystallite size(nm) [W-H plots]**	**Crystallite size(nm) [D-S approach]**	**Strain(x 10^{-4})**
0.5	28	21	1.7
1	28	28	1.8
3	26	27	1.6
5	27	27	1.2
7	27	26	1.5
9	33	25	1.6
11	27	24	1.5

Table 2: Judd-Ofelt intensity parameters (Ω_2, Ω_4), Emission peak wavelengths ($\lambda_p$in nm),radiative transition probability (A_T), calculated radiative (τ_{rad}) lifetime and asymmetric ratio of $YAlO_3$: Sm^{3+} compounds (λ_{ex} = 368 nm).

Tb^{3+} conc. (mol%)	**J–O intensity parameters($\times10^{-20}$ cm^2)**		**Emission peak wavelength λ_p in nm**	**A_T (s^{-1})**	**τ_{rad} (ms)**	**Asymmetric ratio**
	Ω_2	**Ω_4**				
0.5	1.34	1.94	604	12.11	8.25	1.195
1	3.84	3.29	600	34.55	2.89	2.245
3	3.31	2.92	600	29.78	3.35	2.189
5	2.40	2.25	601	21.58	4.63	2.04
7	2.30	2.35	600	20.69	4.83	1.88
9	2.15	2.46	600	19.37	5.16	1.675
11	2.03	1.82	600	18.42	7.25	1.438

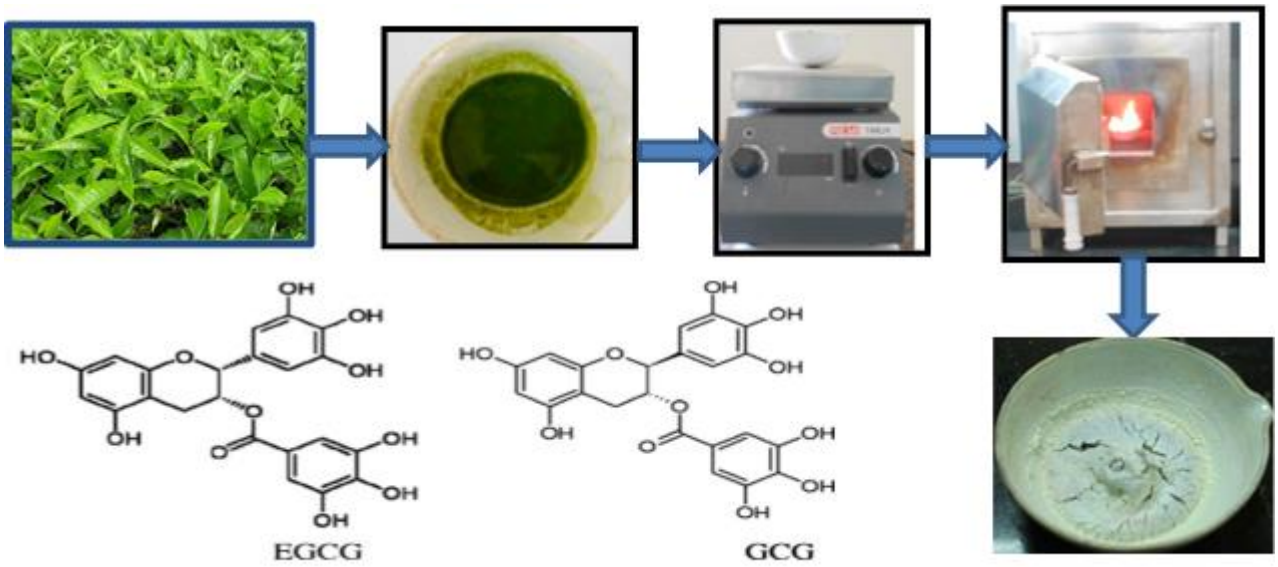

(-)-gallocatechin gallate (GCG, >45%), (-)-Epigallocatechin gallate (EGCG, 36– 40%), (-)-Epigallocatechin (EGC 0.7–2.3%), and (-)-Epicatechin (EC 0.5–2.2%)

Fig. 1 .Flowchart for the preparation of $YAlO_3$: Sm^{3+} nanophosphor and the major chemical contents of green tea.

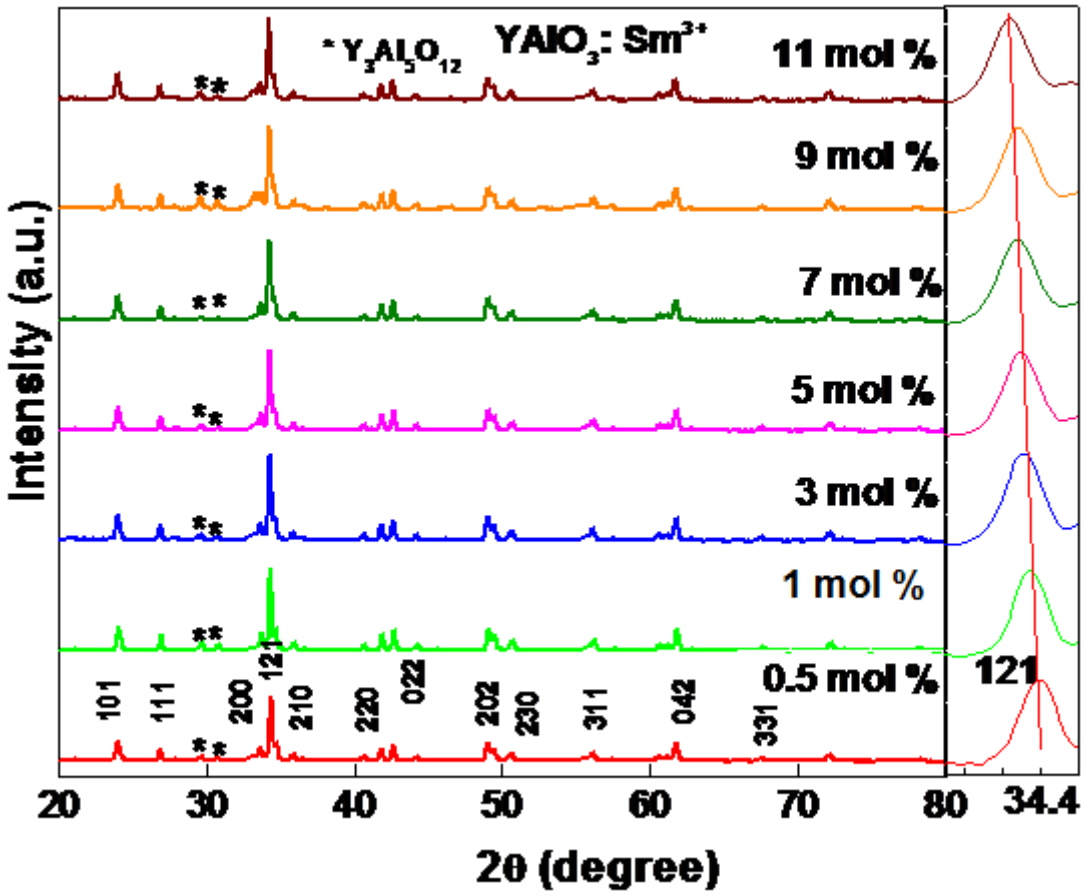

Fig.2. PXRD patterns of (0.5 –11 mol %) Sm^{3+} doped $YAlO_3$ nanophosphor.

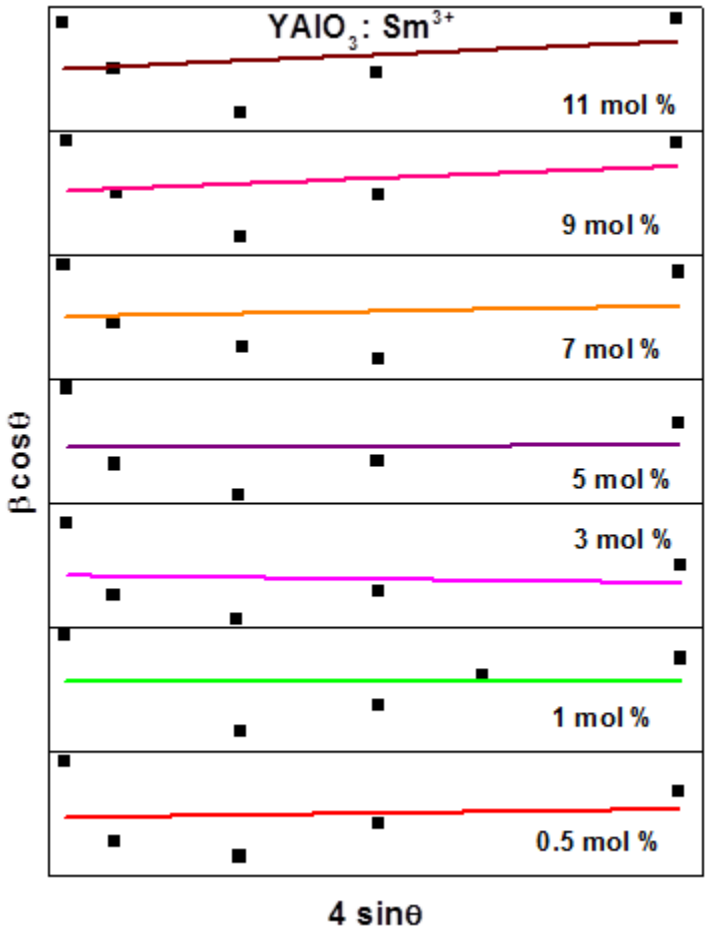

Fig. 3.W–H plots of $YAlO_3:Sm^{3+}$ (0.5–11 mol %).

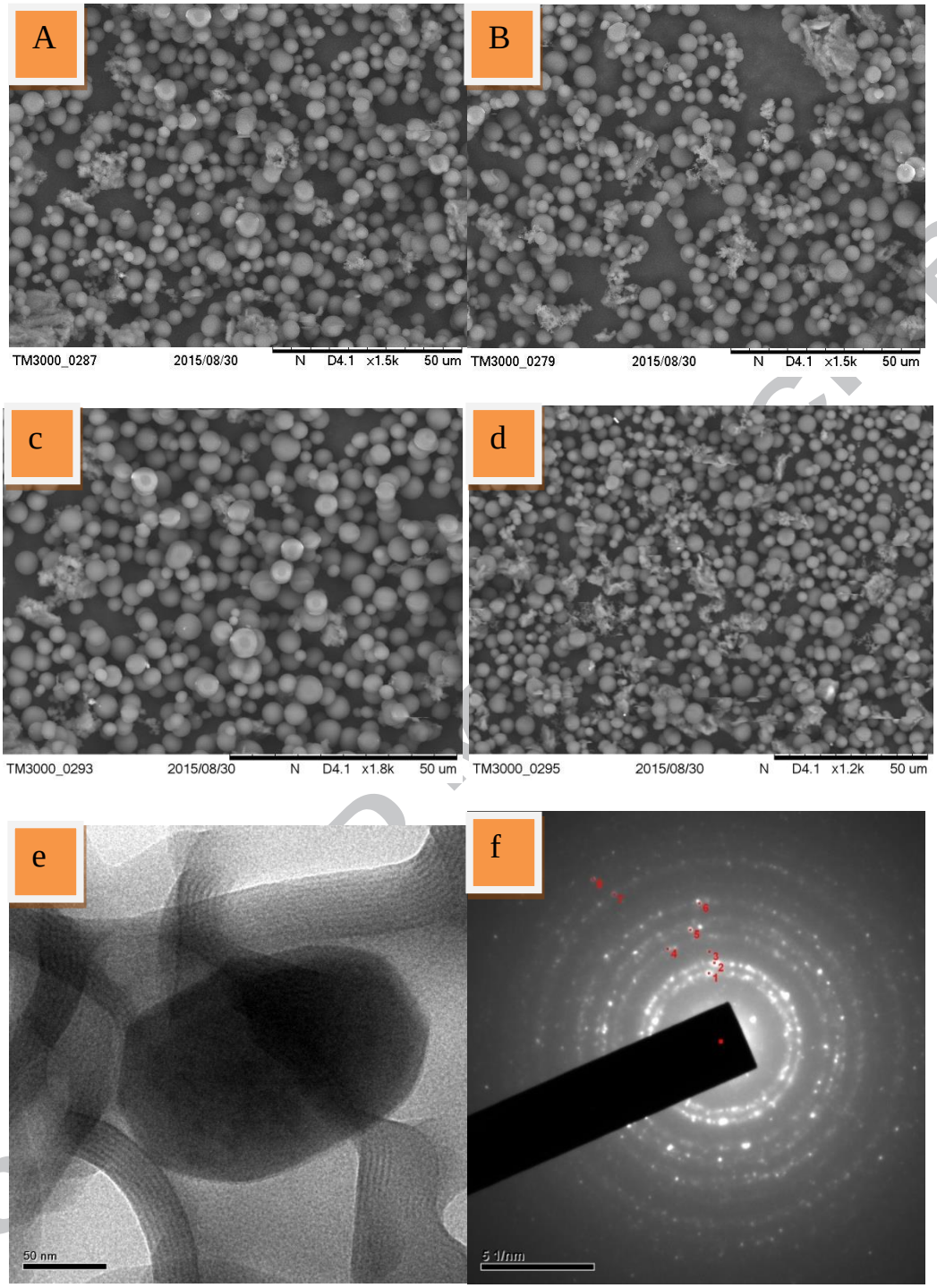

Fig. 4(A–D).SEM micrographs of $YAlO_3:Sm^{3+}$ (1, 3, 7 and11 mol %) nanophosphor, (E and F) TEM and SAED image of $YAlO_3:Sm^{3+}$ (5 mol %).

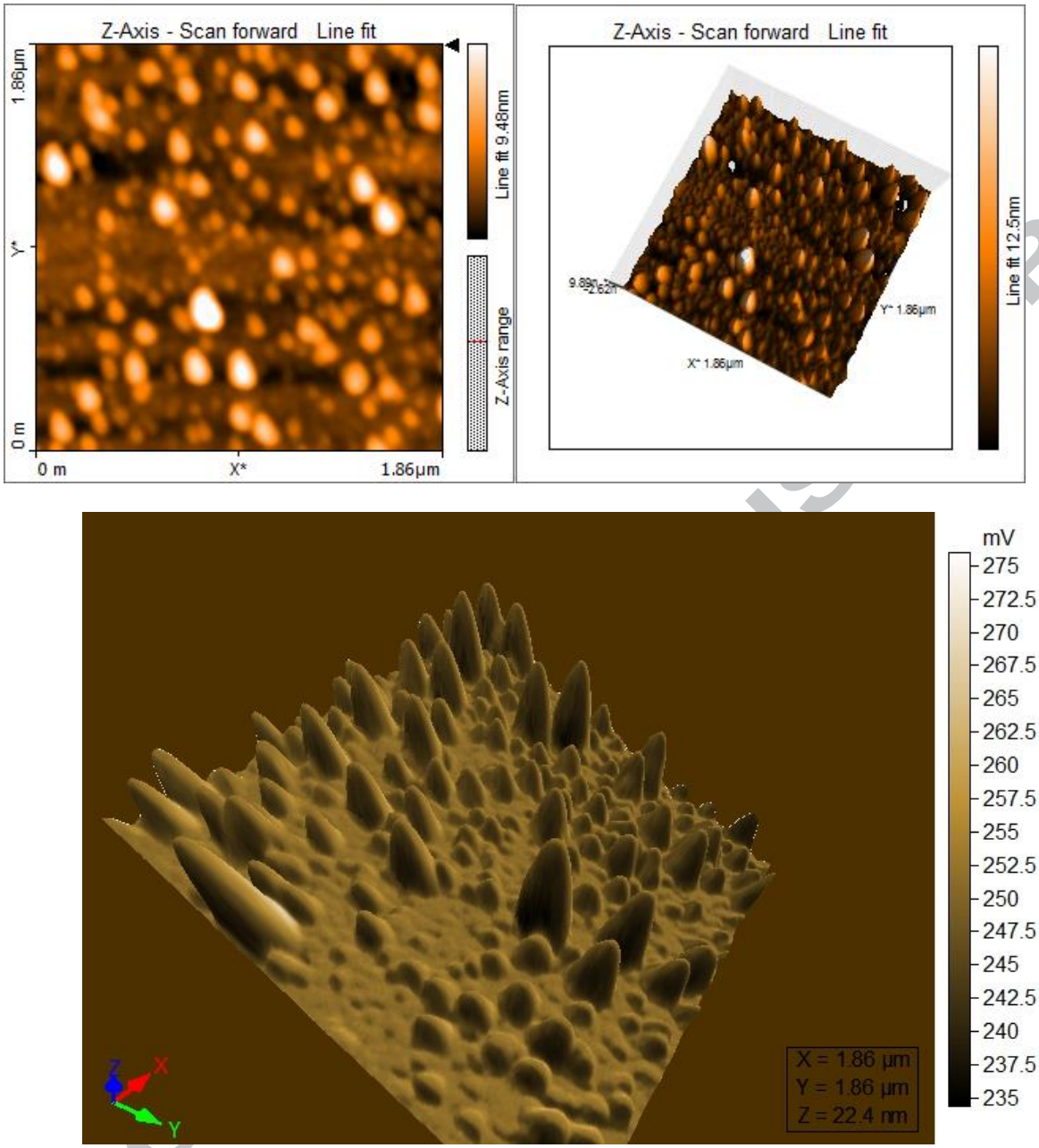

Fig.5. AFM images of 1 mol% Sm^{3+} doped $YAlO_3$ nanophosphor

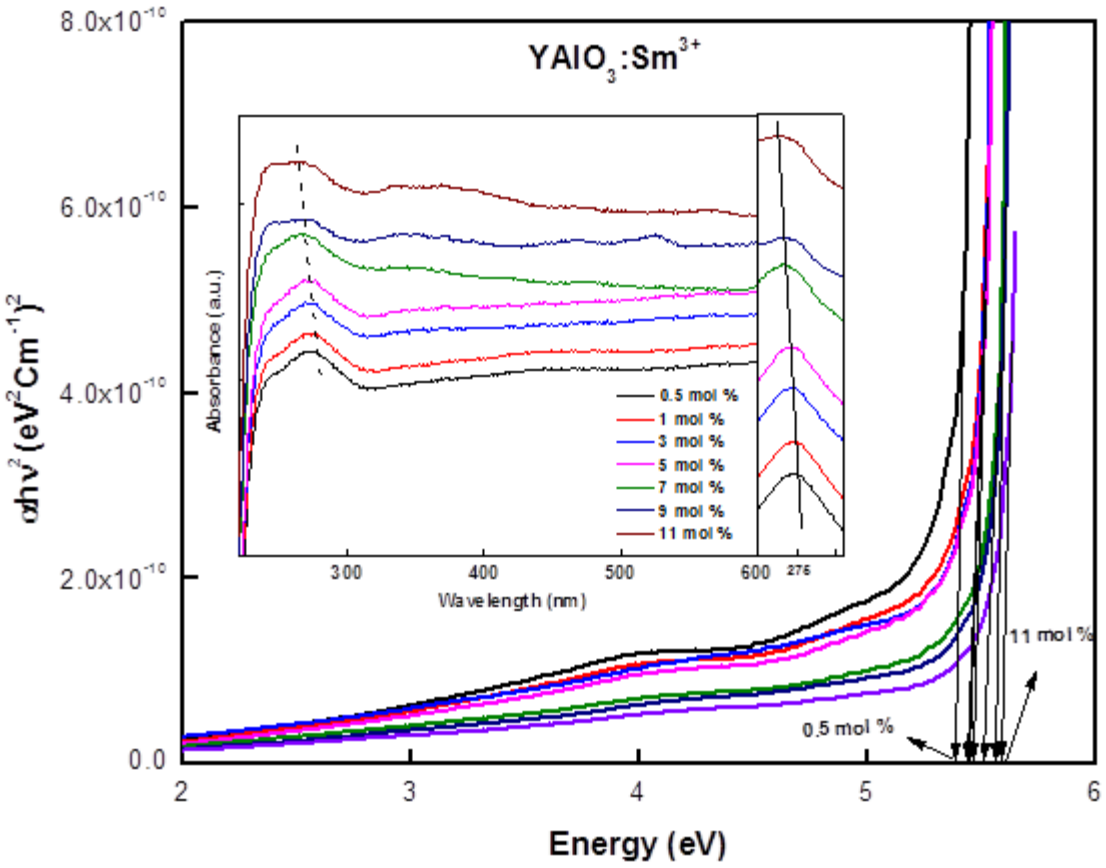

Fig.6.Energy band gaps of (0.5–11 mol %) Sm^{3+} doped $YAlO_3$ nanophosphors.

(Inset: Uv–Vis absorption spectra of (0.5-11 mol %) Sm^{3+}doped$YAlO_3$)

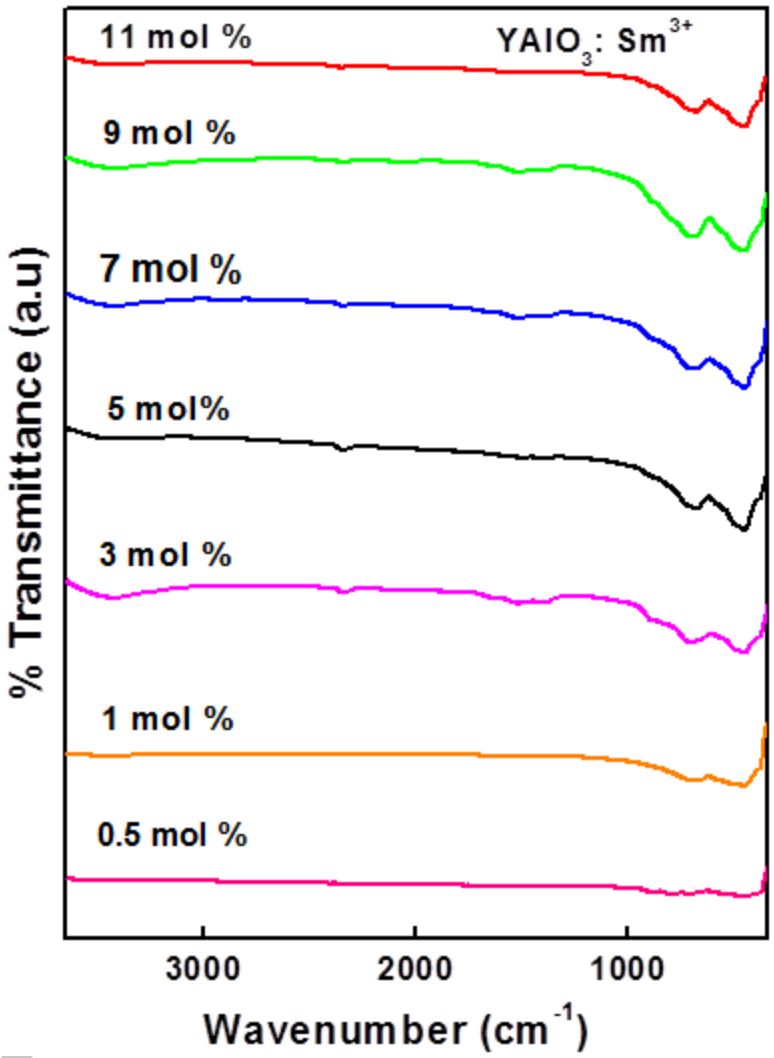

Fig.7. FTIR spectra of $YAlO_3:Sm^{3+}$ (0.5-11 mol %) nanophosphors.

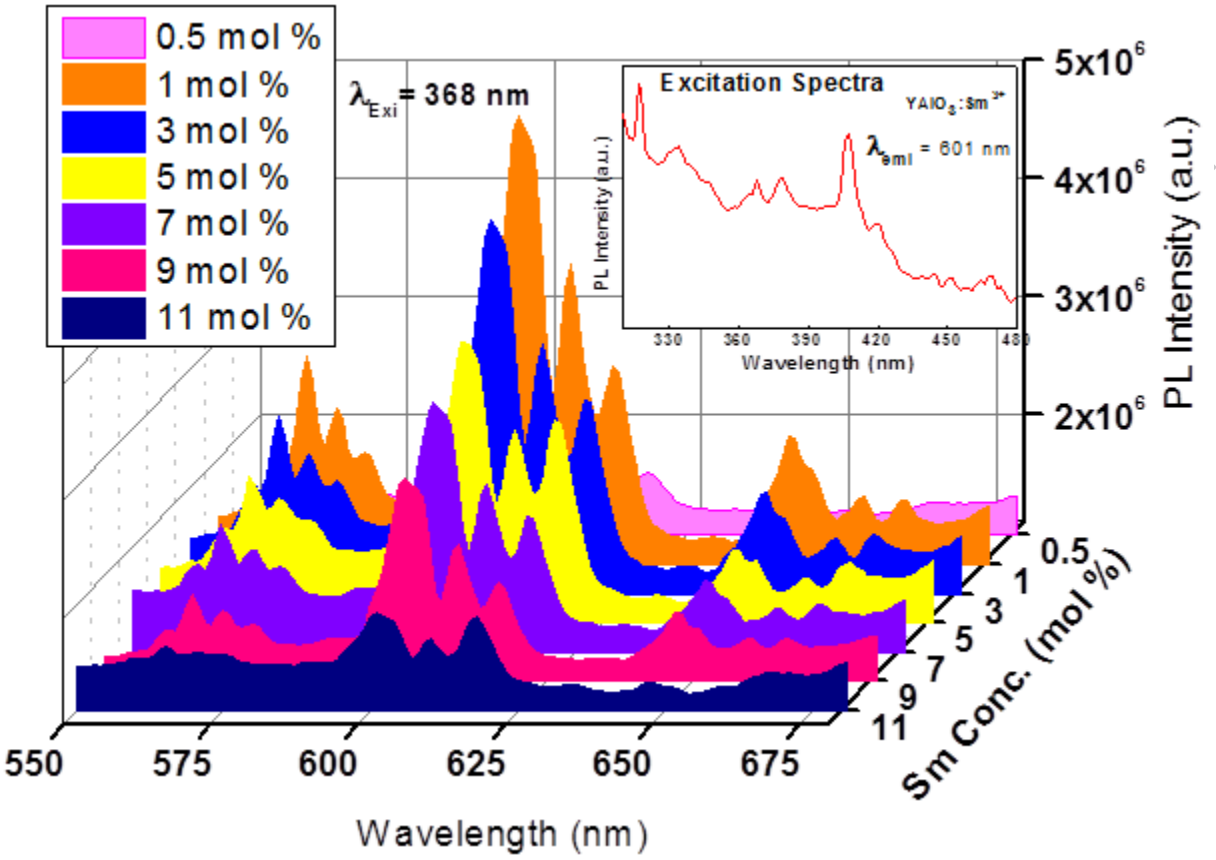

Fig.8. PL spectra of $YAlO_3:Sm^{3+}$(0.5–11mol %) nanophosphors recorded at RT.

(Inset Excitation spectra of $YAlO_3:Sm^{3+}$(11 mol %) at $\lambda_{emi} = 601$ nm)

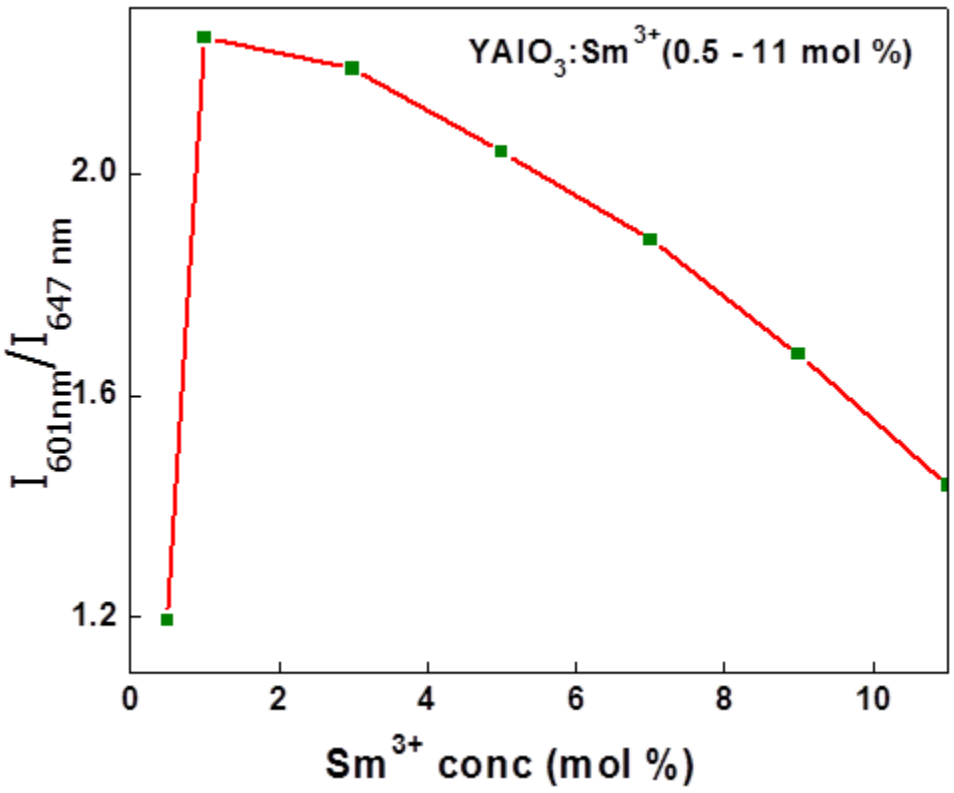

Fig.9. Variation of asymmetric ratio with Sm^{3+}concentration in $YAlO_3$ nanophosphors

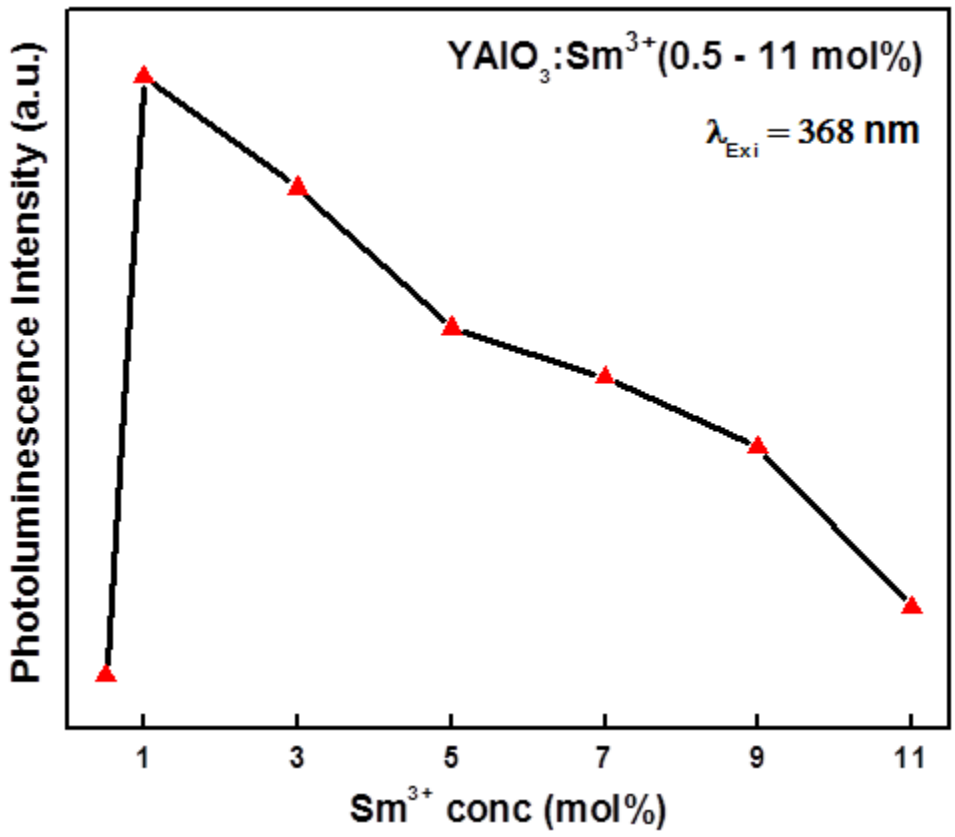

Fig.10. Effect of Sm^{3+}concentration on the 601 nm emission peaks in $YAlO_3$ nanophosphors

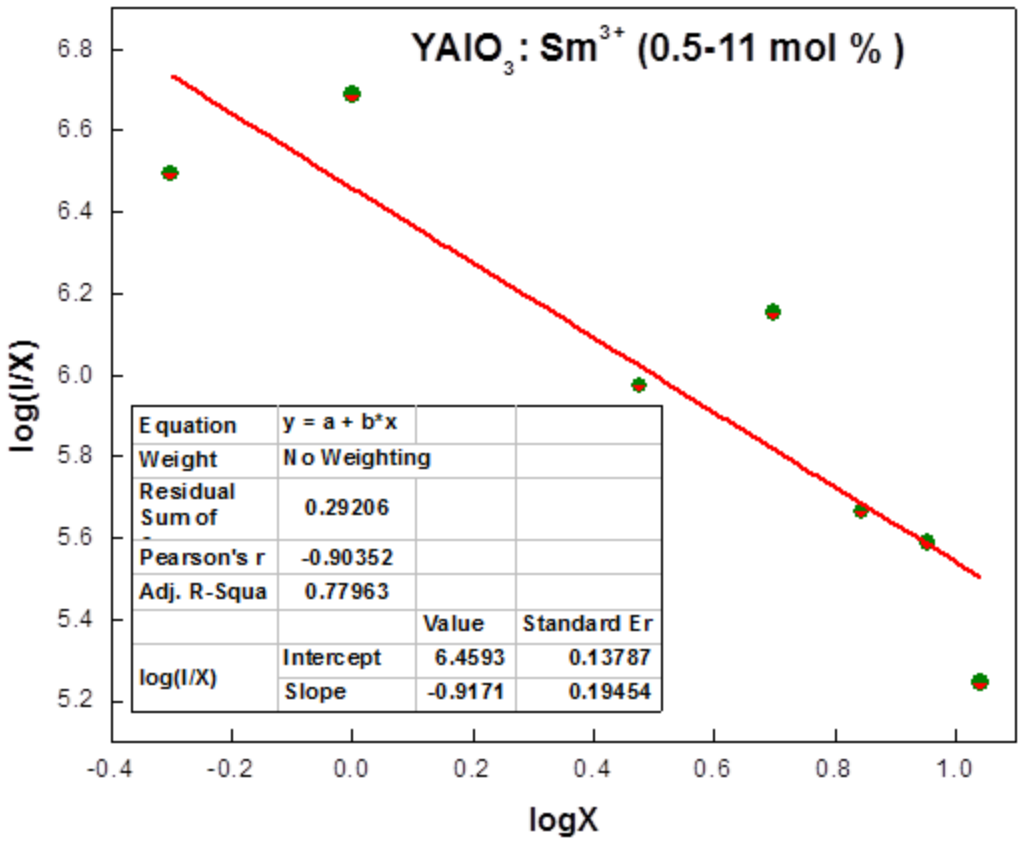

Fig.11. Relation between log(x) and log (I/x) in $YAlO_3:Sm^{3+}$(0.5–11mol %) nanophosphors.

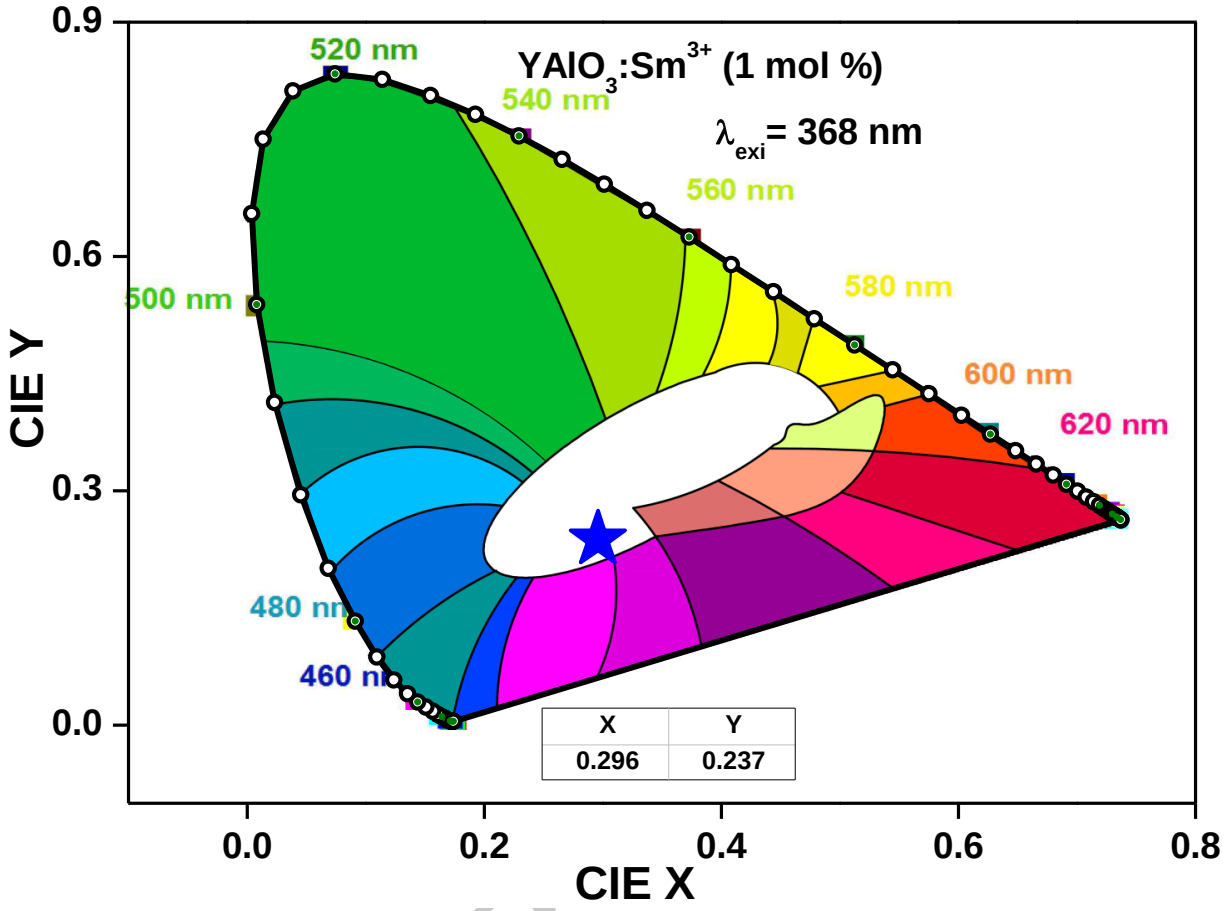

Fig.12. CIE diagram of $YAlO_3:Sm^{3+}$ (1mol %) nanophosphor.

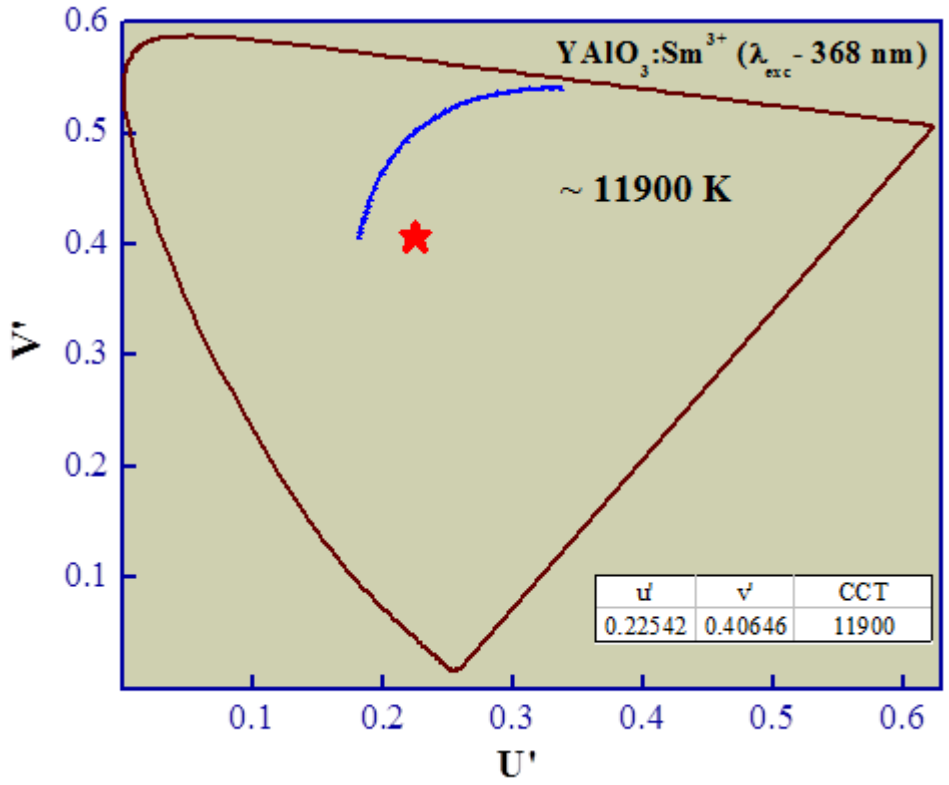

Fig.13. CCT diagram of $YAlO_3$: Sm^{3+} (1 mol %) nanophosphor.

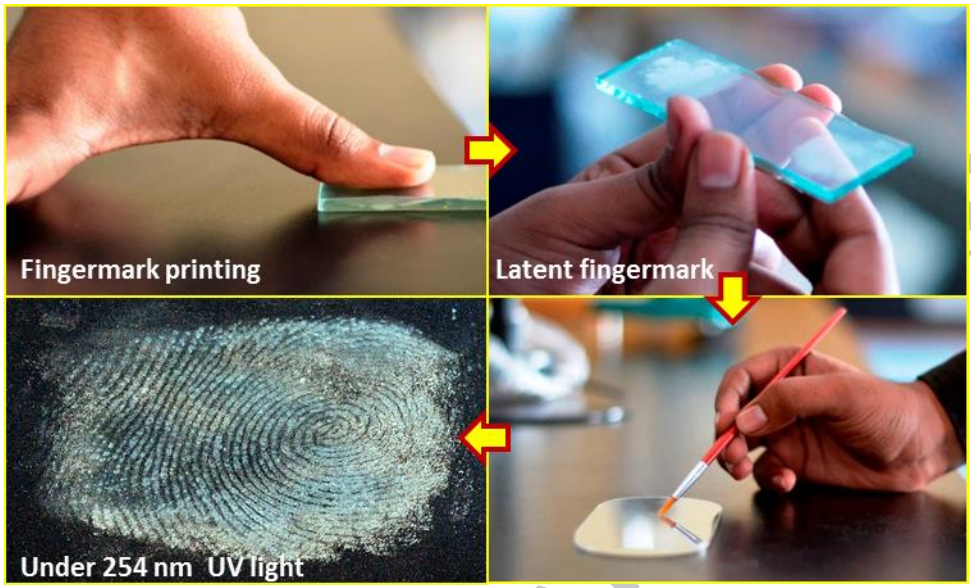

Fig.14. Illustration of the development of latent fingermarks using a $YAlO_3$: Sm^{3+} (1 mol %) nanophosphor dusting process. A fingermark was printed on a glass. Then, $YAlO_3$:Sm^{3+} (1 mol %) nanophosphor powder was deposited onto the substrate to stain the fingermark. A 365 nm UV light was then used to irradiate the fingermark, leading to the excitation of $YAlO_3$: Sm^{3+} (1 mol %) nanophosphor to emit white light and consequently revealing the fingermark with high sensitivity and contrast.

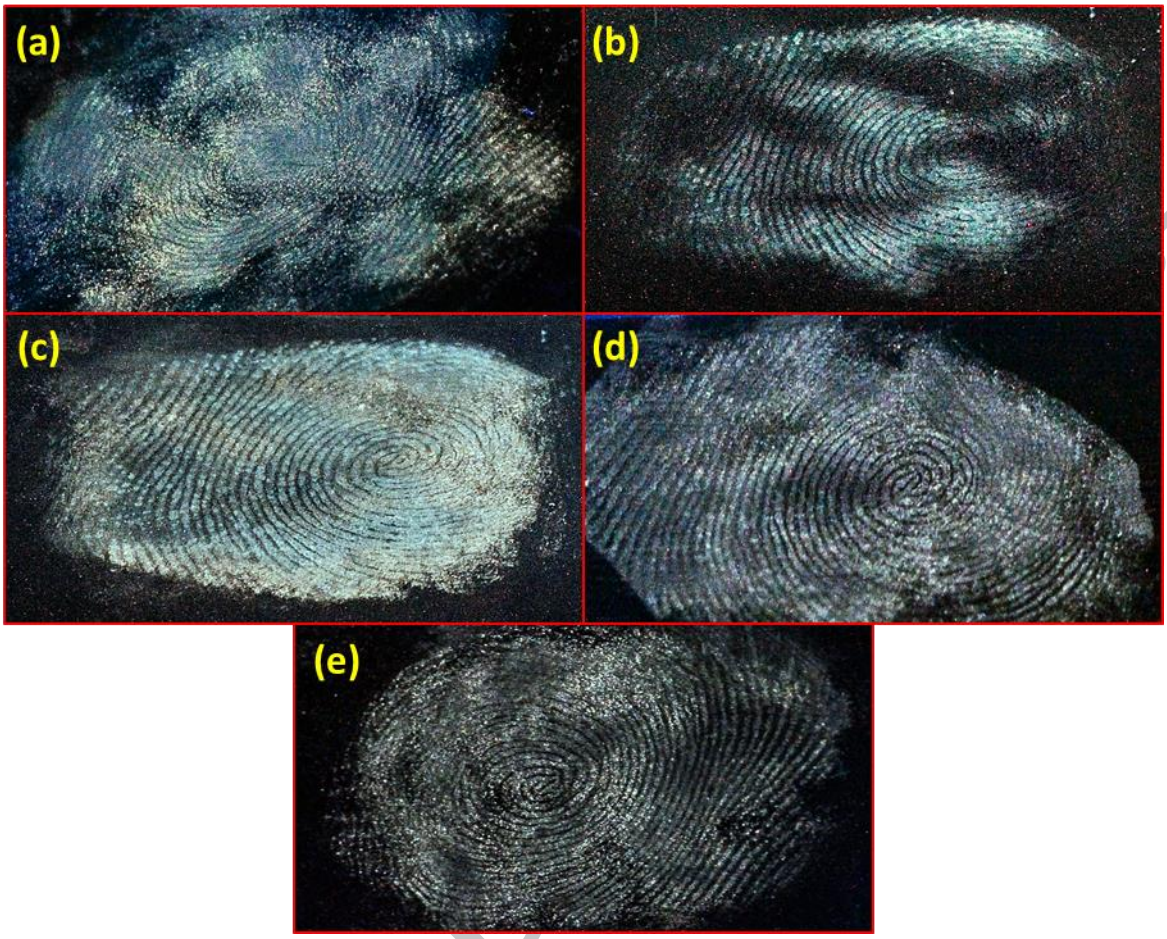

Fig.15. Latent fingermarks stained by $YAlO_3:Sm^{3+}$ (1 mol %) nanophosphor and detected on the surface of various substrates after 365 nm UV light irradiation: (a) aluminum foils (b) Glass (c) transparent plastic sheet (d) stainless steel (e) freshly cut leaf

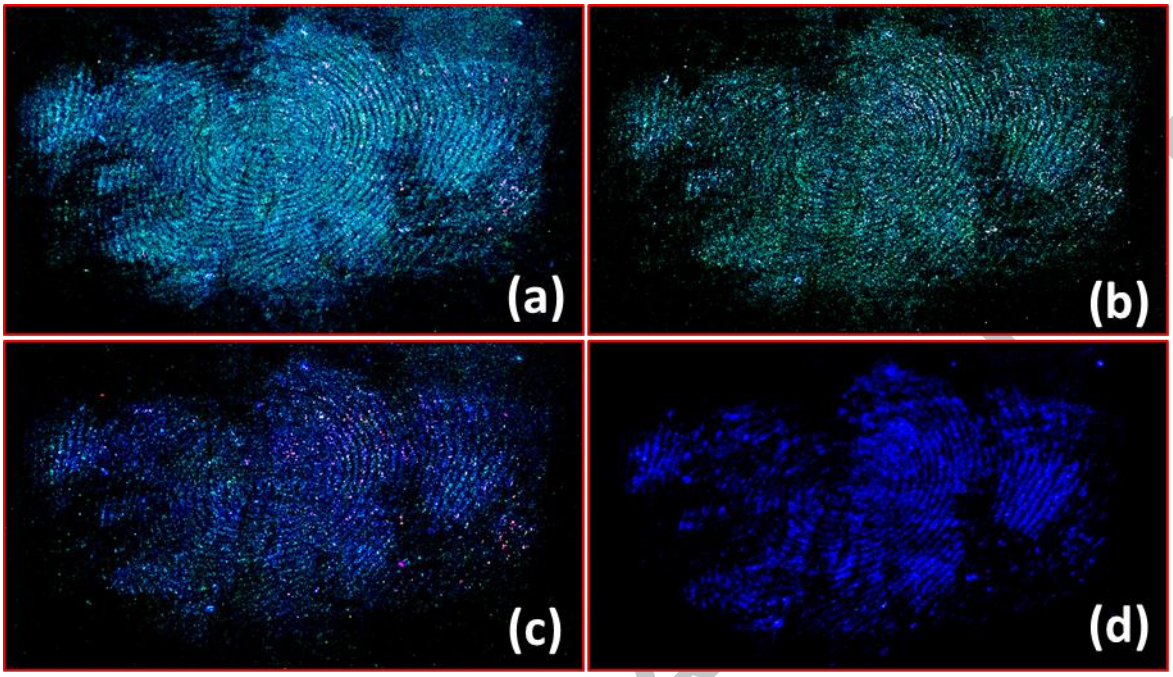

Fig. 16. Latent fingermarks aged on the surface of glass for various periods of time, stained by YAlO3:Sm^{3+} (1 mol %) and finally detected by 365 nm UV light irradiation (a) 1 day (b) 5 days (c) 10 days (d) 30 days

Fig.17. Latent fingermarks stained by $YAlO_3:Sm^{3+}$ (1 mol %) nanophosphor for analysis of correspondences.

Graphical Abstract